Synthesis and Characterization of Catalytic Nanoporous Carbon Membranes

Michael S. Strano and Henry C. Foley
Dept. of Chemical Engineering, University of Delaware, Colburn Laboratory, Newark, DE 19716

A method is reported for the synthesis of novel catalytic nanoporous carbon membranes. Defect-free, nanoporous carbon films of 12.5- μm average thickness containing a dispersion of Pt_x were synthesized on macroporous stainless-steel supports. Ideal gas selectivities for the catalytic membranes were similar to those of inert nanoporous carbon membranes with $He–N_2 = 58.6$ and $O_2–N_2 = 4.9$. The selective hydrogenation of monoolefins (propylene, 1-butene, isobutylene) was used to probe the shape-selective catalytic properties and the transport selectivities of the membranes. The results were modeled using the linear regime of coupled adsorption, transport and reaction in the membrane. Model regression yielded 14.9, 19.7, and 18.4 kJ/mol for the activation energies of permeation for propylene, isobutylene, and 1-butene, respectively. The system demonstrated selective reaction and transport favoring propane production with selectivity ratios of 28.9:3.2:1 for propane:n-butane:isobutane at 125°C.

Introduction

Membrane reactors have generated a great deal of interest for use in the selective catalytic reaction of industrial chemicals. There have been several reviews that point to their potential advantages, including operational savings by increasing conversion, and improved product selectivity (Armor, 1989, 1992, 1998; Saracco and Specchia, 1994; Saracco et al., 1994, 1999). Among other advantages, membrane reactors have the potential to exceed equilibrium conversions by selectively removing species from the reaction zone (Raich and Foley, 1995) or by eliminating undesired pathways in reaction networks (Harold et al., 1993; Raich and Foley, 1998).

Armor (1998) emphasizes the development of highly selective nanoporous membranes for use as membrane reactors, observing that catalysts with larger pores and low transport selectivities require additional downstream separation to recover the product of value. To this end, there have been a number of recent studies exploiting the molecular sieving properties of nanoporous membranes for use in catalytic reactors. Alfonso and coworkers (1999) studied the effects of various feed configurations for propane oxidative dehydrogenation over a V/Al_2O_3 catalytic membrane/zeolite film composite, among other types of hybrid membranes. In this case, however, the intrinsic activity of the zeolite membrane itself suppressed the catalytic selectivity by increasing the overall conversion. Using a supported silicalite-1 membrane, van de Graaf and coworkers were able to demonstrate supraequilibrium conversion in the metathesis of propene (van de Graaf et al., 1999a,b). The membrane selectivity transported *trans*-2-butene over the other species in the reaction zone, thereby augmenting to a small extent the thermodynamic conversion of the reaction from 34% to 38.4%.

Nanoporous carbon (NPC) is a promising material for use as a catalytic membrane in that it is chemically inert under most reaction conditions and thermally stable at temperatures well above 200°C where most industrially relevant reactions occur (Foley, 1995; Kane et al., 1996). Formed from the pyrolysis of nongraphitizing natural or synthetic polymeric precursors, NPC is a disordered material having pores on a scale of molecular dimensions and has been shown to generally possess "shape selective" molecular transport properties (Acharya et al., 1999). Poly-furfuryl alcohol (PFA)-derived nanoporous carbons have a mean pore size of about 0.5 nm, as measured from N_2 and methyl chloride adsorption

Correspondence concerning this article should be addressed to H. C. Foley at this current address: Dept. of Chemical Engineering, Penn State University, University Park, PA 16802.

isotherms (Mariwala and Foley, 1994). Attempts to use this material in the synthesis of defect-free, micron-scale films on structurally stable macroporous supports have been successful. Membranes have been fabricated using NPC that are selective for the separation of small molecular species (Acharya et al., 1997; Acharya and Foley, 1999; Shiflett and Foley, 1999). There have not been to date any studies appearing in the literature using nanoporous carbon in a catalytic membrane reactor.

The purpose of this article is to report a method for the synthesis of novel catalytic NPC thin films for use as catalytic membrane reactors (CMR). In addition to physical characterization, insight regarding the transport properties of the membranes can be obtained using the permeation of selected weakly adsorbing molecular probe gases, for which membranes of this type are known to separate to a significant extent. Additionally, olefin hydrogenation is a simple model reaction system to examine the combined catalytic and transport properties of such membranes.

Background

The selective hydrogenation of olefins has been used by several researchers to characterize the shape-selective behavior of metal on nanoporous carbon catalysts (Trimm and Cooper, 1970, 1973; Schmitt and Walker, 1971a,b; Lafyatis, 1992). Trimm and Copper (1970) polymerized furfuryl alcohol in the presence of H_2PtCl_6, and subsequently pyrolyzed the resulting mixture, creating a Pt/NPC catalyst. The nanoporosity of the catalyst support was shown to contribute to the selective hydrogenation of propene and 1-butene over isobutene, 3-methylbutene, and 3,3-dimethylbutene. Schmitt and Walker (1971a,b) fabricated a similar catalyst and demonstrated shape selectivity between 1-butene and isobutane. Lafyatis (1992) used the conversion ratio of propylene to isobutylene over various NPC-derived metal-supported catalysts to characterize the reactant shape selectivity. These ratios exceeded 14 (propylene/isobutylene) at about 30% conversion of propylene.

Saracco and coworkers (Saracco and Specchia, 1994; Saracco et al., 1994; 1999) assert that an understanding of transport through highly selective, presumably nanoporous media is paramount for the development of catalytic membrane reactors. To this end, the authors of this work have focused on applying the current ideas of transport through these types of media in an attempt to understand the combined effects of transport and selective reaction in this novel reactor configuration. For such a reactive membrane, one can identify essentially two aspects of selective behavior. The membrane itself can be permselective to various reagents and products due to the selective porosity of the material. There is also a shape-selective catalytic effect imposed on the reactant or product in the vicinity of the active site. The nanoporosity of the catalyst-support material can limit the effective surface area of metal of a particular reactant, or prevent a particular transition state or product distribution from existing within the medium. For instance, Miura and coworkers (1993) have argued for transition state selectivity using a 0.4-nm pore size Ni on NPC catalyst in the decomposition of methanol by producing only CO and H_2. This result was attributed to a shape selectivity of the carbon/metal interface that hindered the formation of a transition state yielding methane in the product distribution. Lafyatis and Foley examined methylamine synthesis in solid acid and NPC composite catalysts (Foley et al., 1994), and concluded that transport effects in the carbon led to enhanced yields of the less sterically hindered mono- and dimethylamine.

By applying the current theory for multicomponent transport in nanoporous media (Krishna and Vandenbroeke, 1995; Krishna and Wesselingh, 1997) to selective hydrogenation in a nanoporous carbon membrane, a model can be developed to isolate these separate aspects of selectivity. It can be shown that the decoupling of transport and reaction kinetics for nanoporous systems is a powerful characterization tool to guide in catalytic membrane synthesis and development.

Experiment Studies

Metal catalyst precursor inclusion

Catalytic nanoporous carbon membranes were synthesized using a spray deposition technique that has appeared in the literature. Acharya and coworkers (1997) demonstrated the successful synthesis of highly selective, inert NPC membranes using a deposition technique involving a poly-furfuryl alcohol/acetone precursor (Acharya and Foley, 1999). Previous methods of preparing metal on NPC supports appearing in the literature were not directly adaptable to this method of thin-film formation. Aside from an inability to solubilize PFA, Pt on nanoporous carbon precursors derived from chlorplatinic acid (Schmitt and Walker, 1971a,b; Trimm and Cooper, 1973) led to an unstable solution viscosity, since the polymerization of PFA is known to be acid-catalyzed. Similarly, direct contacting of particulate matter with the NPC precursor, such as solid metal oxides, with diameters on the micron-length scale (Tachibana, 1990), naturally leads to film defects, as the membrane thickness is expected to be commensurate with the particle diameter. By using a Pt metal precursor that is soluble in a PFA cosolvent, these problems are avoided. Furfuryl alcohol resin (Monomer Polymer & Dajac Laboratories Inc., Lot A-1-143), PFA, was added to an equal amount by weight of an acetone solution containing a measured amount of Pt (II) acetylacetonate ($Pt(C_5H_7O_2)_2$) (97% purity; Strem Chemicals) in order to achieve the desired metal loading. This method allowed the introduction of the catalytic metal with little impact on the established deposition methodology.

Membrane preparation

The catalytic membranes were prepared by attaching a sintered metal stainless-steel support (0.1-μm pore size, 11.4-cm^2 area) obtained from Mott Metallurgical Co. to a rotating shaft at 30 rpm and spray coating with approximately 10 mg/cm^2 of polymer solution (Acharya and Foley, 1999). The resulting system was subsequently pyrolyzed in a stream of flowing He at 5°C/min to 500°C, held for 2 h at this temperature, and then allowed to cool to room temperature. This deposition process was repeated three times until a mass of approximately 5 mg/cm^2 of nanoporous carbon was deposited on the support and the membrane demonstrated gas selectivities higher than the Knudsen values. Table 1 summarizes the typical parameters for the support and carbon membrane.

Table 1. Membrane and Support Parameters

Support	
Material	316 stainless steel
External Area	11.4 cm^2
Mean pore size	0.2 μm
Thickness	0.8 mm
Porosity	0.6 m^3 void/m^3 support
Membrane	
Thicknesses	12.5 μm
Deposition mass	5 mg carbon/cm^2
Number of coats	3 coats
Catalytic loading	1.32% Pt/C
Density of carbon	1.6 g/cm^3
Synthesis Temp.	500 °C
Soak Time	2 h
Heating ramp rate	5°C/min
He purge flow rate	50 std. cm^3/min

Scanning electron microscopy

Membrane cross sections were cut orthogonal to the carbon layer using a diamond-wafering saw. These sections were mounted in an epoxy resin, polished, and given a coating of Au for imaging with a Hitachi S-4000 field-emission scanning electron microscope. Imaging and EDAX were performed on areas of this cross section external to and within the macroporosity of the stainless-steel support and at various radii from the center of the disk-shaped membranes.

Transmission electron microscopy

Bulk Pt on carbon samples were also prepared by pyrolyzing the catalytic precursor in PFA resin, grinding and dividing it to 140/230 mesh. These granular samples were suspended in ethanol and deposited on TEM backings for imaging after evaporation of the solvent to more effectively determine metal size distributions. Metal loadings were determined by elemental analysis at Galbraith Laboratories Inc. (Knoxville, TN).

Molecular probe transport

Transport of H_2, He, N_2 and O_2 was used to characterize the selective porosity and integrity of carbon film. The disk-shaped membranes were sealed using Viton gaskets into a stainless-steel module set up to measure the transport of a single gas through the membrane. At a time $t = 0$, the probe gas was introduced to the top of an initially evacuated membrane at a pressure p_o. The permeate volume bounding the bottom of the membrane was sealed from vacuum at this time and the subsequent rise in pressure was used to evaluate the instantaneous derivative of the time-dependent flux through the membrane:

$$\frac{V_{pc}}{RT}[P(t) - P_{\text{init}}] = A\int_0^t N(t')\,dt', \tag{1}$$

where V_{pc} is the volume of the permeate chamber, P_{init} is the initial pressure in the chamber at $t = 0$, and A is the area of the membrane. This pressure was measured using an MKS Baratron pressure transducer (0–1,000-torr range) and recorded using an interfaced PC that also controlled the start and duration of the experiment via electronically actuated solenoid valves. If the pressure rise in this volume is not permitted to exceed a minimum value, then the driving force across the membrane is essentially equal to the pressure loading. In this way, the steady-state flux of the molecular probe can be measured as a function of the driving force pressure, p_o.

Effective membrane thickness

The membrane layer exists partially external to and within the macroporosity of the stainless-steel support and, hence, has an effective thickness that cannot be determined directly through microscopy. As with other supported nanoporous membranes, the membrane/support interface was typically dominated by cracks and irregularities (Yamamoto et al., 1997; van de Graaf et al., 1999d). A phenomenological, effective thickness of the membrane layer can be measured using the method of Strano and Foley (2000). Taking helium ($p_0 >$ 101 kPa; $T > 298.15$ K) to be essentially nonadsorbing upon the nanoporosity of the membrane, the transient response of the permeate flux to a step change in He pressure loading can be used to calculate the effective thickness, δ, via

$$\delta = \frac{6N_{ss}\tau RT}{p_o}. \tag{2}$$

Here N_{ss} is the steady-state flux of He through the membrane at a driving-force pressure of p_o, and τ is the extrapolated time axis intercept of the transient integral molar flux at steady state. Due to voids within the carbon layer, the thickness measured in this way is typically between 30% and 50% of the thickness calculated from the mass of carbon and its density (Strano and Foley, 2000).

Catalytic testing

Selective hydrogenation of olefins has been used by several authors to characterize the shape-selective catalytic behavior of metal on NPC catalysis (Schmitt and Walker, 1971a,b; Trimm and Cooper, 1973; Schmitt, 1991):

$$\text{Olefin} + H_2 \rightarrow \text{Alkane}.$$

Figure 1 is a diagram of the experimental setup used to benchmark the catalytic membranes using this particular re-

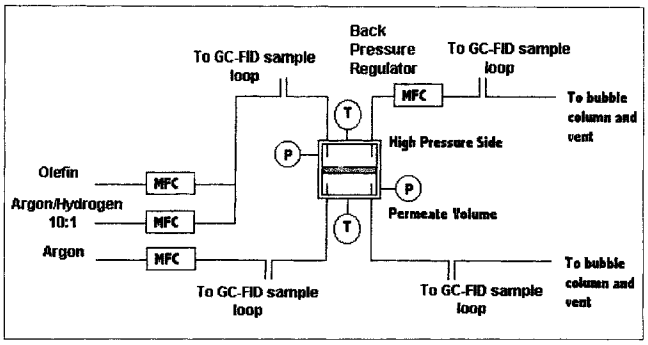

Figure 1. Experimental setup used to conduct the selective hydrogenation.

action system. A 100:10:1 mixture of argon:hydrogen:olefin was fed to one side of the membrane, while an argon sweep carried the permeate fluxes out from the temperature and back-pressure-controlled reactor. The use of an argon diluent in the feed and as a sweep gas suppresses its driving force across the membrane, and hence allows the total flux through the membrane to be dominated by only the species of interest for dilute reactants and products. All streams entering and exiting the reactor module were sampled using a Varian 3700 Gas Chromatograph with an FID detector and a 23% SP-1700 on 80/100 Chromosorb P AW column. The conversion was defined as

$$x_{\text{olefin}} = \frac{A_{\text{alkane}} R_{\text{alkane}}}{A_{\text{alkane}} R_{\text{alkane}} + A_{\text{olefin}} R_{\text{olefin}}}, \tag{3}$$

where A and R are the measured area and response factor of the species indicated exiting the reactor in the permeate sweep and raffinate streams.

The catalytic membrane was reduced in a flowing stream of a 80-sccm argon/hydrogen mixture (10:1) at 200°C for 12 h. This extended treatment had the additional advantage of purging the membrane of any adsorbed hydrocarbons trapped within the porosity of the membrane in between hydrogenation runs.

Hydrocarbons adsorb onto NPC carbon to a significant extent and display transport that is strongly temperature and concentration dependent (see "Selective Hydrogenation" below). Generally, the diffusivity of an adsorbing species decreases to a minimum in the limit of an infinitely dilute adsorbed phase loading. This nonlinearity in the transport coefficient creates a time scale for the achievement of a steady state through the membrane at conditions used in this work that can be on the order of 8–32 h for the olefins.

Using a pulse-injection flow reactor, Trimm and Cooper (1973) observed that temperatures in excess of 600°C were required to desorb residual hydrocarbons completely from a Pt on NPC catalyst. Using the method described earlier for purging the NPC membrane, coupled with the long times required to reach a steady state, essentially no hysteresis was observed in the generation of conversion data with increasing and decreasing temperature, and reproducibility was within experimental limits. The potential for background activity from the stainless-steel support was checked using a noncatalytic NPC membrane at the same reactive conditions, but none was observed.

Selective Hydrogenation: Henry's Law Adsorption, Transport and Reaction

Transport through nanoporous media has been described accurately by the Stefan-Maxwell formalism for multicomponent surface diffusion (Krishna and Wesselingh, 1997; Krishna et al., 1998, 1999; Burggraaf, 1999; van den Broeke et al., 1999; van de Graaf et al., 1999c). For strongly adsorbing molecular probes, the mechanism of transport through this type of medium is one of surface adsorption onto the membrane, followed by transport of the adsorbed phase through the porosity. The Fickian diffusivity matrix for a mixture of N components can be represented as the product of intrinsic or Stefan-Maxwell diffusivities (Krishna and Wesselingh, 1997), $\underline{\underline{D}}$, and a thermodynamic factor, $\underline{\underline{\Gamma}}$, that takes into account the strong concentration dependence and coupling of the Fickian transport coefficient matrix, $\underline{\underline{D}}^{\text{Fick}}$ (assuming Langmuir adsorption):

$$\underline{\underline{D}}^{\text{Fick}} = \underline{\underline{D}} \cdot \underline{\underline{\Gamma}} \tag{4}$$

$$\Gamma_{ij} = \delta_{ij} + \frac{\theta_i}{\theta_v}. \tag{5}$$

$$\theta_v = 1 - \sum_{i=1}^{N} \theta_i. \tag{6}$$

Here, θ_i is the fractional adsorbed phase loading of species i ($\theta_i = q/q_{\text{sat}}$), and θ_v is the fraction of vacant sites, which is an artifact of the finite number of adsorption sites available in the given medium. For the purposes of adsorption and transport through nanoporous membranes, several researchers (Burggraaf, 1999; van den Broeke et al., 1999; van de Graaf et al., 1999c) have utilized the Langmuir adsorption isotherm, yielding for θ_i in this case:

$$\theta_i = \frac{b_i p_i}{1 + \sum_{j=1}^{N} b_j p_j}. \tag{7}$$

Conducting the hydrogenation such that the fractional loadings of the reactant olefin and product alkane are small, the nonlinear coupling between species is predicted to vanish, since

$$\theta_{\text{olefin}}, \theta_{\text{alkane}} \ll 1.$$

Furthermore, hydrogen, like other permanent gases, is expected to adsorb only weakly onto the membrane:

$$\theta_{\text{hydrogen}} \ll 1.$$

In this limit, we note that $\theta_v \approx 1$ and Γ approaches a diagonal, unity matrix. Intuitively, under these conditions one would expect that the presence of the adsorbing hydrocarbon and olefin have no effect on their mutual transport, or on the weakly adsorbing hydrogen. Hence, the transport of all species becomes uncoupled and Fickian in this limit, and the catalytic behavior of the reactants can be observed in the absence of nonlinearities in the transport.

A differential mass balance on the adsorbed phase reactants of the catalytic membrane can be written:

$$q_{\text{sat},i} \epsilon \rho \frac{\partial \theta_i}{\partial t} = \frac{\partial}{\partial z}\left(q_{\text{sat},i} \epsilon \rho D_i \frac{\partial \theta_i}{\partial z} \right) + r_i. \tag{8}$$

Using the definition of θ_i and the simplifications just observed, the mass balance can be written in terms of the bulk

pressure:

$$q_{\mathrm{sat},i}\epsilon\rho b_i\frac{\partial p_i}{\partial t}=\frac{\partial}{\partial z}\left(q_{\mathrm{sat},i}\epsilon\rho b_i D_i\frac{\partial p_i}{\partial z}\right)+r_i. \tag{9}$$

The olefin is in an environment of excess hydrogen, hence one anticipates that the intrinsic reaction rate will be pseudo-first-order with respect to the olefin partial pressure within the membrane:

$$r_i=-k\rho w p_i. \tag{10}$$

Here, w is the metal loading per volume of membrane, and k is the pseudo-first-order rate constant. The boundary conditions at steady state for the feed and permeate volumes bounding the membrane are imposed assuming perfect back mixing in these volumes:

$$\begin{aligned} p_i(z=0)&=p_{h,i}\\ p_i(z=\delta)&=p_{l,i}. \end{aligned} \tag{11}$$

Defining a dimensionless diffusional coordinate, η, and the Thiele modulus for this system below:

$$\eta=\frac{z}{\delta}\qquad \phi_i^2=\frac{\delta^2 kw}{q_{\mathrm{sat},i}\epsilon D_i b_i}, \tag{12,13}$$

the problem in the membrane at steady state becomes

$$\frac{d^2p_i}{d\eta^2}=\phi_i^2 p_i. \tag{14}$$

Solving Eq. 14 and applying the boundary conditions, Eq. 11 yields the bulk pressure profile across the membrane:

$$p_i(\eta)=p_{h,i}\cosh(\phi_i\eta)+\frac{p_{l,i}-p_{h,i}\cosh(\phi_i)}{\sinh(\phi_i)}\sinh(\phi_i\eta). \tag{15}$$

The flux of the reactant can be obtained by evaluation of the derivative of Eq. 15:

$$N_i(\eta)=-\frac{q_{\mathrm{sat},i}\rho\epsilon D_i}{\delta}\frac{\partial\theta_i}{\partial\eta}=-\frac{q_{\mathrm{sat},i}\rho\epsilon D b_i\phi_i}{\delta}\times\left[p_{h,i}\sinh(\phi_i\eta)+\frac{p_{l,i}-p_{h,i}\cosh(\phi_i)}{\sinh(\phi_i)}\cosh(\phi_i\eta)\right]. \tag{16}$$

At the high-pressure boundary ($z=0$), the olefin flux is

$$N_i(\eta=0)=-\frac{q_{\mathrm{sat},i}\rho b_i\epsilon D\phi_i}{\delta}\left[\frac{p_{l,i}-p_{h,i}\cosh(\phi_i)}{\sinh(\phi_i)}\right]. \tag{17}$$

At the permeate boundary ($z=\delta$), the olefin flux is

$$\begin{aligned} N_i(\eta=1)&=-\frac{q_{\mathrm{sat},i}\rho\epsilon D b_i\phi_i}{\delta}\times\left[p_{h,i}\sinh(\phi_i)+\frac{p_{l,i}-p_{h,i}\cosh(\phi_i)}{\sinh(\phi_i)}\cosh(\phi_i)\right]\\ &=-\frac{q_{\mathrm{sat},i}\rho\epsilon D b_i\phi_i}{\delta\sinh(\phi_i)}\left[p_{l,i}\cosh(\phi_i)-p_{h,i}\right]. \end{aligned} \tag{18}$$

From the preceding, the alkane product flux—or amount of alkane generated per unit area—can be calculated as the difference between these two steady-state fluxes in Eqs. 17 and 18,

$$\begin{aligned} N_{\mathrm{alkane}}&=N_i(\eta=0)-N_i(\eta=1)\\ &=-\frac{q_{\mathrm{sat},i}\rho\epsilon D_i b_i\phi_i}{\delta\sinh(\phi_i)}\left[1-\cosh(\phi_i)\right](p_{l,i}+p_{h,i}). \end{aligned} \tag{19}$$

The conversion is defined as the product alkane flux divided by the entering olefin flux:

$$x_{\mathrm{olefin}}=\frac{\left[1-\cosh(\phi_i)\right](p_{l,i}+p_{h,i})}{p_{l,i}-p_{h,i}\cosh(\phi_i)}. \tag{20}$$

If a sweep gas is used to constantly remove the product fluxes from the permeate volume, the partial pressure of the olefin and alkane will be negligible at this boundary. We observe that in this limit, the conversion becomes independent of reactor pressure and a function only of the Thiele modulus:

$$x_{\mathrm{olefin}}=\frac{\cosh(\phi_i)-1}{\cosh(\phi_i)}. \tag{21}$$

Hence, under these conditions, the Thiele modulus for this system can be obtained directly and provides an independent measure of the shape-selective catalytic effects of the membrane.

Results and Discussion

Physical characterization

Figures 2a and 2b are scanning electron micrographs of a catalytic membrane cross section prepared as described earlier. The spray-coating methodology yields a fairly uniform surface coating of carbon upon the support (Figure 2a). Figure 2b reveals that the carbon membrane film extends to a significant extent into the macroporosity of the stainless-steel support. The effective thickness of the selective layer cannot be determined by microscopic methods alone, and a phenomenological definition has been shown to be more appropriate. Using He permeation at 298 K, an average value of 8.2 s was measured for the time intercept at 561-, 350- and 740-kPa driving forces and 1.01×10^{-10} mol/m^2/s/Pa for the He permeance. This corresponds to an effective thickness of about 12.5 μm using Eq. 2.

Figure 3 is an EDAX taken of the carbon adjacent to the support/membrane interface. The loading of Pt used in this

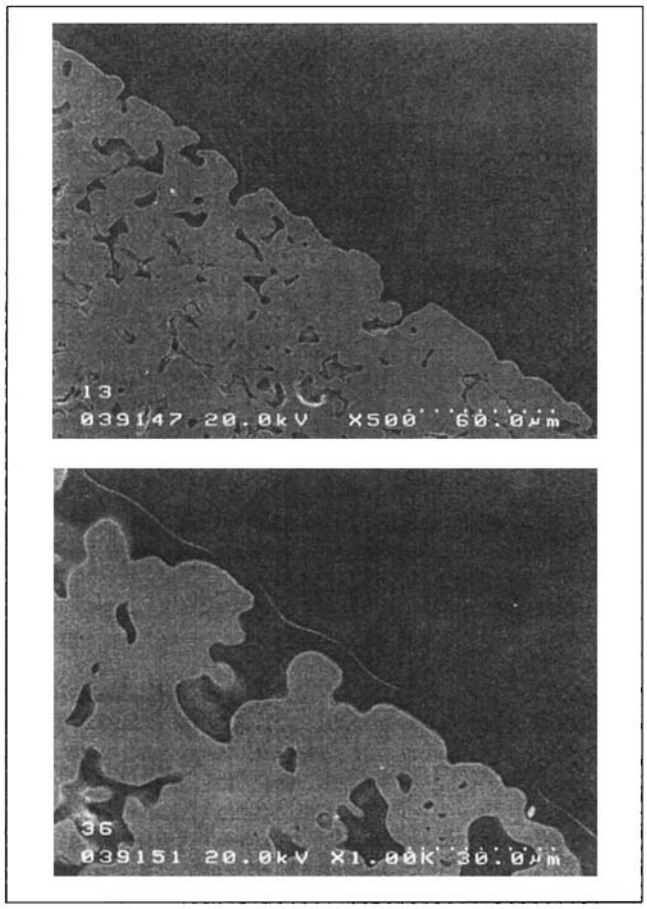

Figure 2. Scanning electrons of catalytic membrane cross sections: (a) uniformity of the carbon layer; (b) extent of penetration into the macroporous support.

study is below the amount required to present a measurable cross section to the electron beam, and hence does not appear in the resulting spectrum. The Au peak is attributed to the preparation method described earlier. Na and O are impurities in the carbon, the former being residual NaOH used

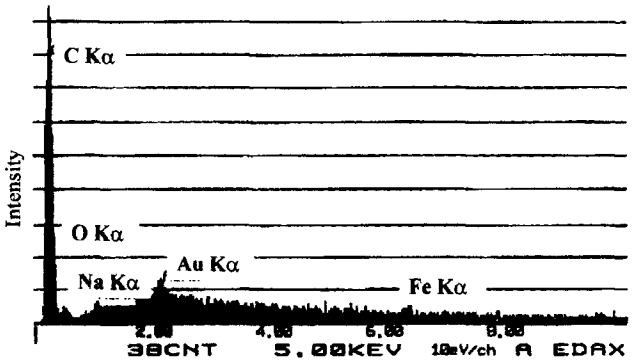

Figure 3. EDAX spectrum of a catalytic membrane cross section around the surface of the support/external layer interface.

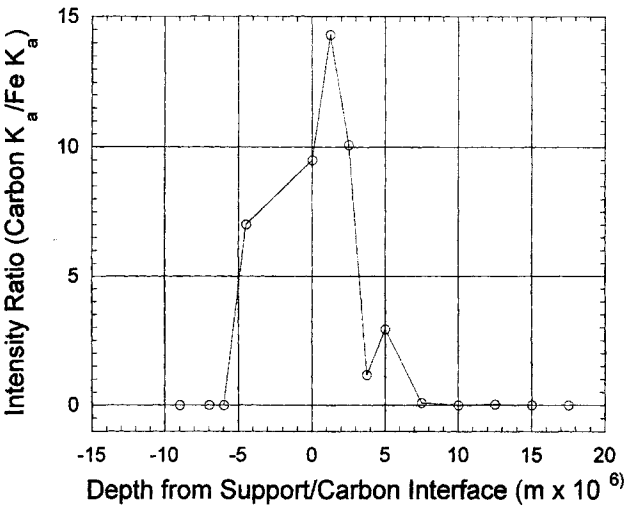

Figure 4. Relative intensity of C to Fe from EDAX as a function of penetration depth from the support surface.

to quench the acid catalyzed polymerization of the furfuryl alcohol monomer, and the latter due to oxygen containing product gases from pyrolysis. Since the carbon layer extends into the macroporous support and the C K_{alpha} to Fe K_{alpha} ratio can be measured as a function of distance from the support interface and averaged along the membrane surface. This yields an indication of the approximate penetration depth and external thickness. Figure 4 presents this surface-averaged intensity ratio with the zero at the support/external carbon interface.

Catalytic dispersion

Figure 5 is a transmission electron micrograph of the unsupported catalytic membrane material. The Pt metal particles, having diameters of less than 10 nm, are visible within the carbon support as indicated. A histogram of metal diameters was obtained from a series of such micrographs. The results obtained with a sampling of 200 particles are displayed in Figure 6. Defining a volume-averaged mean diameter where n_i and d_i are the number and diameter of each particle in the sample set,

$$d_{\text{vol}} = \frac{\sum_i n_i d_i^3}{\sum_i n_i d_i^2},$$

yields a value of 7.1 nm. As the number of particles is rather low, d_{vol} yields only a rough indication of the mean particle size. The unweighted average of the distribution was calculated as 3.0 nm. The measured dispersion using the synthesis methodology above was observed to be consistently higher than that measured for a Pt/NPC material derived from H_2PtCl_6. Lafyatis (1992) found the Pt dispersion of such materials to be independent of the pyrolysis temperature of the carbon and approximately 4.6 nm (unweighted average). Pt

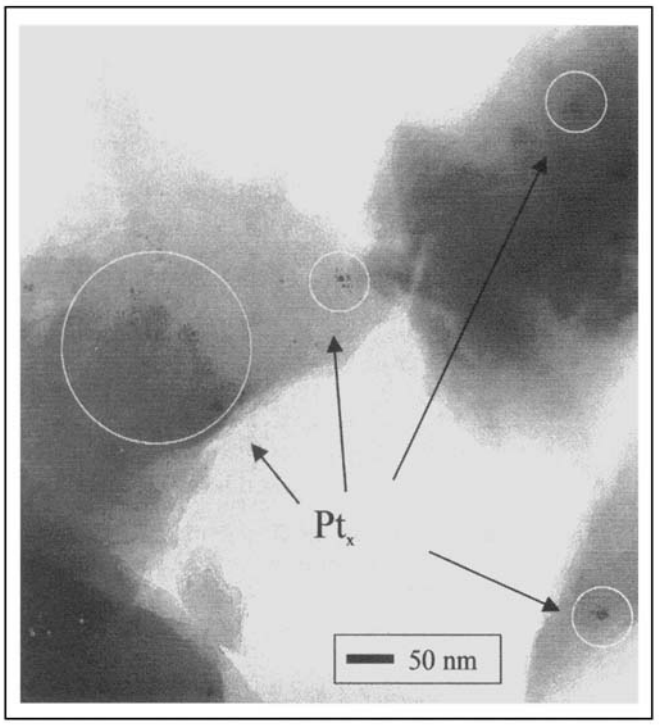

Figure 5. TEM of Pt catalyst on the nanoporous carbon support.

(II) acetylacetonate, being soluble in the PFA cosolvent, apparently does not agglomerate to the extent that a H_2PtCl_6 does, possibly because of the absence of the aqueous phase. Although Reyes and coworkers (1996) studied a fundamentally different synthesis technique, they observed similar Pt precursor effects in the synthesis of Pt on alumina catalysts.

Molecular probe transport

Figure 7 presents the steady-state fluxes vs. driving force pressure across a catalytic membrane for H_2, He, O_2, and N_2. The linearity observed as well as the high ideal separation factors (calculated as the ratio of slopes) indicate that the membranes are defect free. Defects or surface cracks that span the thickness of the active layer reduce separation factors significantly and create a quadratic dependence of the flux vs. pressure typical of viscous flow. As with their inert analogs, there is strong evidence of shape-selective transport, as the separation factors for these molecular probes are quite high ($He-N_2 = 58.6$; $O_2-N_2 = 4.9$) despite minimal differences in the kinetic diameter of the molecular probes.

There is no evidence that the presence of the metal significantly affects the transport properties of the NPC membrane. The permeances and separation factors reported in Figure 7 are typical for a carbon layer of the indicated thickness and synthesis conditions (Acharya et al., 1997).

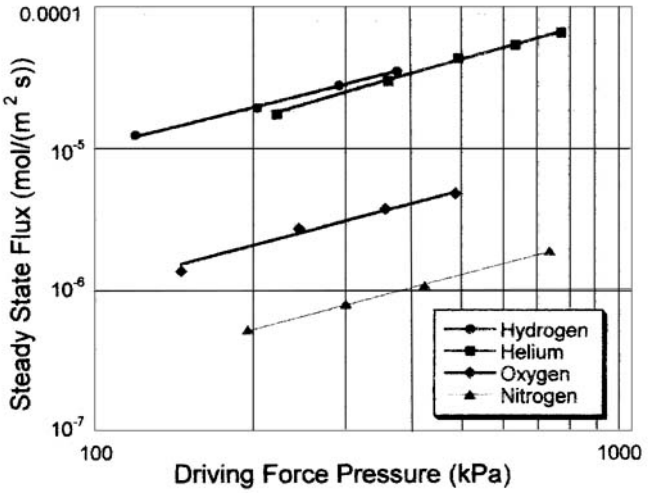

Figure 7. Steady-state flux at 298 K through a catalytic nanoporous carbon membrane as a function of driving-force pressure.

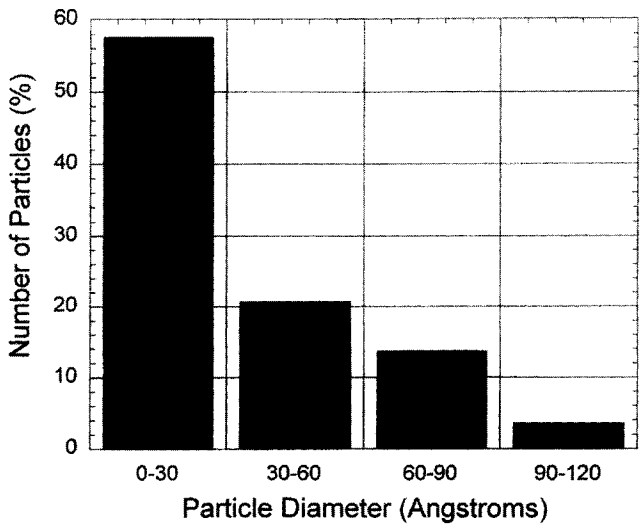

Figure 6. Particle-size distribution of Pt on nanoporous carbon.

Hydrogenation model validation

For a given feed composition, as the hydrogenation temperature increases, the extent of reactant adsorption onto the membrane is expected to diminish and move into the Henry's law portion of the isotherm. In this regime, the model derived in the previous section is expected to be valid. Similar behavior could be expected if the concentration of olefin in the reactor feed was to be reduced. Figure 8 is the propylene conversion as a function of the feed partial pressure in the reactor volume above the membrane and parametric in temperature for a 10-to-1 hydrogen-to-propylene feed. This partial pressure was controlled by manipulating the total back pressure in the reactor on the feed side of the CMR from 101 to 350 kPa. As the hydrogenation temperature increases, the conversion becomes independent of the reactor pressure, as demonstrated. Because the volumetric flow rate of the argon sweep through the permeate chamber is large compared to the fluxes through the membrane, the concentrations of the permeate gases in the sweep remain close enough to zero, and Eq. 21 can be used to calculate the Thiele modulus un-

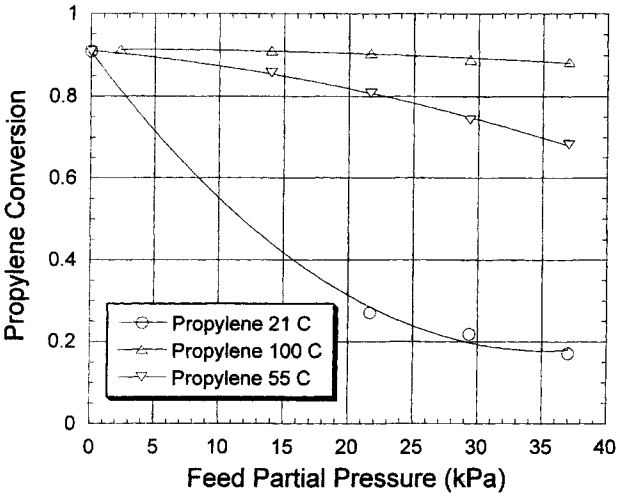

Figure 8. Conversion vs. feed partial pressure for propylene parametric in reactor temperature.

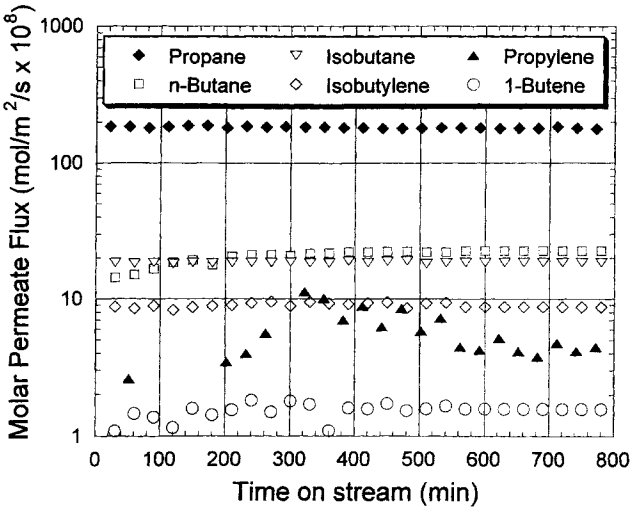

Figure 10. Transient hydrogenation fluxes for propylene, isobutylene, and 1-butene as a function of time on stream at 100°C.

der these conditions. Similar behavior for the conversion vs. temperature and reactor partial pressure was observed for 1-butene and isobutylene.

Further evidence for being within this linear hydrogenation regime is that at elevated temperatures (> 100°C) the reactant and product permeate fluxes become directly proportional to the partial-pressure driving force of the reactant in the feed to the CMR. Hence the observed fluxes are in agreement with Eqs. 16–18 for the case where the partial pressures approach zero in the permeate chamber. Figure 9 demonstrates this behavior for the case of propylene hydrogenation at 100°C.

Catalytic testing

Figures 10 presents the time-on-stream behavior of the catalytic membrane permeate fluxes after achieving steady-state conditions at 125°C and 102-kPa total pressure. Propane is the favored hydrogenation product with almost complete conversion and a selectivity ratio of 28.9:3.2:1 for propane:*n*-butane:isobutane. This figure confirms the absence of irreversible membrane fouling or catalyst deactivation over a time scale of 800 min. The same conclusion was reached for all data points over the temperature range tested. The variability in the propylene and 1-butene permeate fluxes is attributed only to detector noise, as conversions for these two reactants were exceedingly high.

Figures 11–13 are the resulting feed and permeate fluxes from hydrogenation over a range of temperatures from 40°C to 175°C at a partial pressure of 1.0 kPa of olefin to the feed side of the CMR. At temperatures above 125°C, 1-butene isomerization to *cis*- and *trans*-2-butene occurs at conversions greater than 1%, and for this reason, the 1-butene hydro-

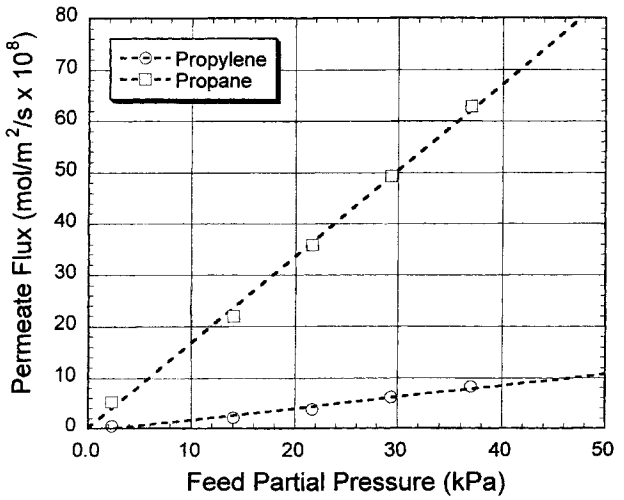

Figure 9. Steady-state hydrogenation fluxes of propane and propylene as a function of driving-force pressure at 100°C.

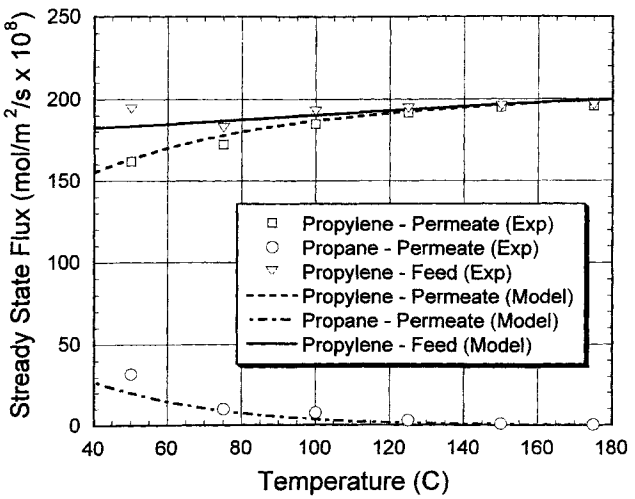

Figure 11. Experimental and model-predicted steady-state hydrogenation fluxes for propylene as a function of reactor temperature.

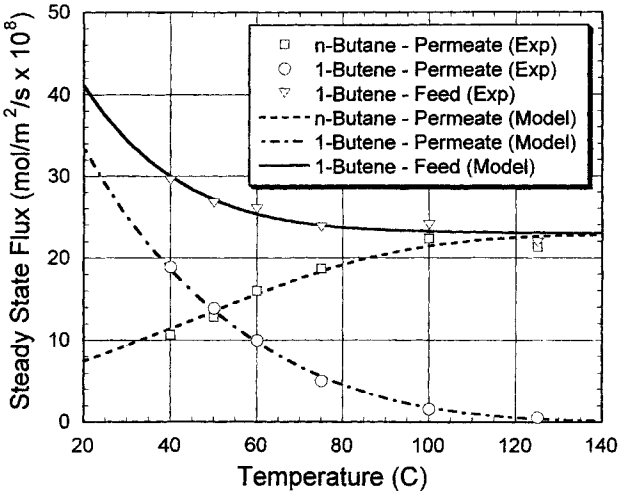

Figure 12. Experimental and model-predicted steady-state hydrogenation fluxes for 1-butene as a function of reactor temperature.

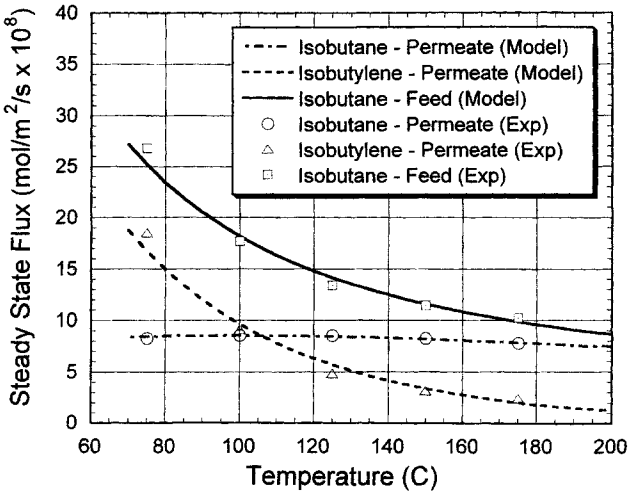

Figure 13. Experimental and model-predicted steady-state hydrogenation fluxes for isobutylene as a function of reactor temperature.

genation data ranges only from 40° to 125°C. The propylene and propane fluxes are generally about a factor of 10 higher than the C_4 components, as is evident from a comparison of Figure 11 with Figures 12 and 13. It is also apparent that propylene and 1-butene conversions to the product alkane are higher than that of isobutylene over the entire temperature range. The hydrogenation model developed in the previous section can be applied in rationalizing these observed trends.

The Thiele modulus for the hydrogenation system can be obtained from the conversion data using 21. The pseudo-first-order hydrogenation rate constant, defined by Eq. 10, is

$$k_i = k_i^o \exp\left(-\frac{E_{r\times n,i}}{RT}\right). \tag{22}$$

Similarly, the Langmuir adsorption constant and surface diffusivity are similarly temperature dependent:

$$D_i = D_i^o \exp\left(-\frac{E_{sur,i}}{RT}\right) \tag{23}$$

$$b_i = b_i^o \exp\left(\frac{\Delta H_{ads,i}}{RT}\right). \tag{24}$$

From Eqs. 22 through 24, the anticipated temperature dependence of the Thiele modulus can be derived:

$$\ln(\phi_i) = \frac{1}{2}\ln\left(\frac{\delta^2 k_o w}{q_{sat,i} b_i^o \varepsilon D_i^o}\right) + \frac{1}{2}\frac{(-E_{r\times n,i} - \Delta H_{ads,i} + E_{sur,i})}{RT}. \tag{25}$$

Figure 14 is a plot of $\ln(\phi_i)$ vs. the inverse hydrogenation temperature and is linear for all hydrocarbons tested, as Eq. 25 predicts. The slopes and intercepts from this plot can be used to obtain the groups of activation and preexponential parameters. These parameters are summarized in Table 2.

Equation 17 can be used in conjunction with the knowledge of ϕ_i to calculate the transport coefficients for the three olefins:

$$q_{sat,i}\,\rho b_i \varepsilon D_i = q_{sat,i}\,\rho b_i^o \varepsilon D_i^o \exp\left(\frac{\Delta H_{abs,i} - E_{sur,i}}{RT}\right) = \frac{N_i(\eta = 0)\sinh(\phi_i)\delta}{\phi_i \cosh(\phi_i) p_{h,i}}. \tag{26}$$

Table 2. Results of Parameter Regression of Combined Transport and Kinetic Data

	$q_{sat} b_i^o \epsilon \rho D_i^o$ mol/(m·Pa·s)	$k_o w\rho/(q_{sat}\,\rho b_i^o \epsilon D_i^o)$ (1/m^2)	$\Delta H_{abs,i} - E_{sur,i}$ kJ/mol
Isobutylene	2.66×10^{-18}	1.24×10^{13}	19.69
1-Butene	2.32×10^{-18}	8.11×10^{15}	18.41
Propylene	3.78×10^{-17}	2.11×10^{15}	14.90
	$E_{r\times n,i} - \Delta H_{abs,i} - E_{sur,i}$ kJ/mol	$E_{r\times n,i}$ kJ/mol	K_o mol/(s·Pa·g Pt)
Isobutylene	22.08	2.39	0.0000328
1-Butene	36.33	17.92	0.0188
Propylene	29.39	14.49	0.0799

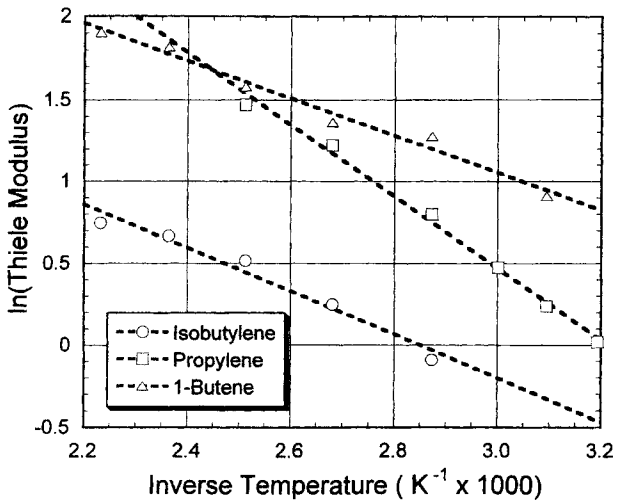

Figure 14. Thiele modulus for hydrogenation as a function of reactor temperature as obtained from conversion measurement.

The parameter δ is 12.5 μm for this particular catalytic membrane, as measured using the technique just discussed. In a manner similar to Figure 14, Figure 15 can be used to obtain the activation and preexponential parameters pertaining to olefin transport, and these values are summarized in Table 2. The values obtained for the quantity $\Delta H_{\text{abs},i} - E_{\text{sur},i}$ in this way are all positive, and demonstrate an increasing trend with increasing carbon number, as is typically found for nanoporous carbon adsorbents (Chihara et al., 1978) and zeolite membranes (Burggraaf, 1999). The values for the overall permeabilities of propylene are an order of magnitude higher than those of the C_4 hydrocarbons and all fluxes decrease with temperature (Figure 15).

Taking the log of Eq. 26 and subtracting Eq. 25 from this twice yields an expression for the activation energy and A-factor for the hydrogenation rate constant, and these values are presented in Table 2. The known catalytic loading of

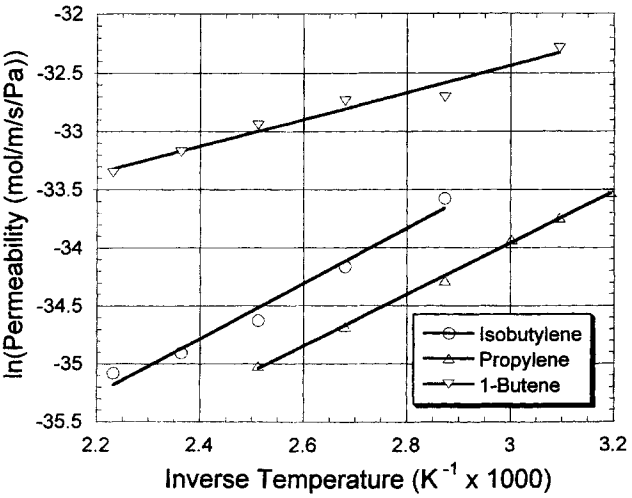

Figure 15. Permeability as a function of reactor temperature for the hydrogenation system.

0.0132 (kg Pt/kg catalytic membrane) and a value of 1.6 kg/m^3 for the density of the nanoporous carbon were used.

Figure 17 compares the rate constants for the three olefins calculated in this way. The apparent kinetic selectivity represented as the ratio of rate constants is more than 62.8 for propylene/isobutylene and 5.3 for 1-butene/isobutylene at 125°C. The latter value is significantly higher than the intrinsic ratio of 1.9 reported by Lafyatis (1992), who also estimated an analogous, diffusion-limited ratio of 13.3 for hydrogenation over a granular Pt/NPC catalyst for these reactants. Lafyatis assumed, however, that transport within the molecular sieving carbon could be represented using a simple effective diffusivity and linear driving force. Hence, adsorption effects and the concentration dependence of the diffusivity were not fully accounted for at lower temperatures and higher adsorbed phase loadings.

A plausible explanation for the considerable differences in apparent hydrogenation rates is that reaction and transport through the membrane may not occur homogeneously throughout the bulk of the carbon. Rather, the formation of the carbon film can give rise to an isotropic pore structure within the membrane. A small population of Knudsen transport pathways or "defects" would possess lower mass-transport resistance and yield a disproportionate control of the membrane flux. This possibility has been relatively unexplored in many studies of carbon membranes and may account for the fact that O_2/N_2 separation factors for these membranes have varied considerably with preparation method: from 4.9 (this work) to 30 (Shiflett and Foley, 1999).

The substantial variation in the kinetic selectivities then comes about because reaction occurs in parallel with transport across the membrane—not homogeneously within the carbon film. Figure 17 contrasts the differences in the pore structures for both models. Taking into account the potentially isotropic nature of the medium, the rate constants reported earlier are still not intrinsic, but remain disguised in the classic sense by diffusion limitations. The results therefore suggest that the carbon exerts a significant amount of reactant shape selectivity, and this is consistent with the findings of other studies involving nanoporous carbon catalysts (Schmitt and Walker, 1971a,b; Trimm and Cooper, 1973; Lafyatis and Foley, 1990).

The idea of critical pathways dominating the reaction and transport through the membrane is not unlike the case of silicalite-1 and other zeolite-based nanoporous membranes where crystal growth produces distinct grain boundaries. Flow through these membrane defects occurs in parallel with adsorption and transport onto the nanoporosity of the medium (van de Graaf et al., 1999d). In this way, a zeolite-based catalytic membrane is expected to demonstrate similar apparent kinetic behavior to that observed in this work. For the case of nanoporous carbon, a natural consequence of this concept is that there exists considerable opportunity to improve the selectivities of these types of catalytic membranes as new synthesis approaches are developed, leading to fewer defect pathways.

Conclusions

A method for the synthesis of novel supported catalytic nanoporous carbon membranes was presented for use as a

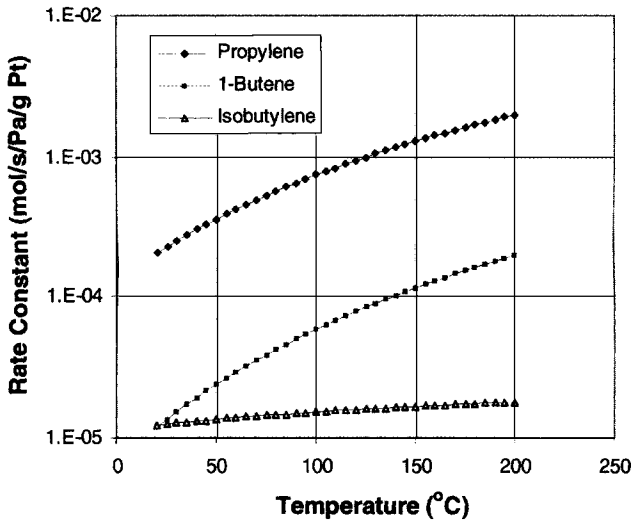

Figure 16. Intrinsic hydrogenation rate constants vs. temperature from model regression.

permselective catalytic membrane reactor (CMR). The method produces selective thin carbon films with the catalytic metal dispersed within the membrane layer. Scanning electron micrographs reveal that the membrane structure exists both within and external to the macroporosity of the stainless-steel support. The effective thickness of these membranes from He permeation measurements is $\sim 12.5\ \mu$m. The Pt metal dispersion as estimated via TEM on membrane material was observed to have a volume-averaged metal diameter of 7.1 nm. Selective hydrogenation of monoolefins demonstrated the utility of the selective transport porosity of the membrane as well as the shape-selective catalytic effects.

The catalytic membranes demonstrated good selectivity in the hydrogenation of olefins, as measured as a ratio of product fluxes with 28.9:3.2:1 for propane:*n*-butane:isobutane at 125°C. The ratios of observed hydrogenation rate constants measured for this system are larger than expected based on intrinsic rates determined for other Pt catalysts: 62.8 and 5.3 for propylene/isobutylene and 1-butene/isobutylene. These results can be rationalized in terms of the anisotropic nature of the membrane material. One consequence of this observation is that there exists considerable opportunity to improve the selectivities of these types of catalytic membranes as new synthesis approaches are developed, leading to membranes with fewer defect pathways.

Acknowledgments

This work was supported by the Department of Energy, Office of Basic Energy Sciences; the Delaware Research Partnership; and the E.I. duPont deNemours and Co., Inc. The authors appreciate the help of Dr. R. Li and J. Pedrick at DuPont Central Research & Development for TEM and JEM imaging, respectively.

Notation

A = area of membrane, m^2
A_{alkane} = alkane chromatography peak area
A_{olefin} = olefin chromatography peak area
b_i = Langmuir parameter for species i for adsorption on a carbon membrane Pa^{-1}

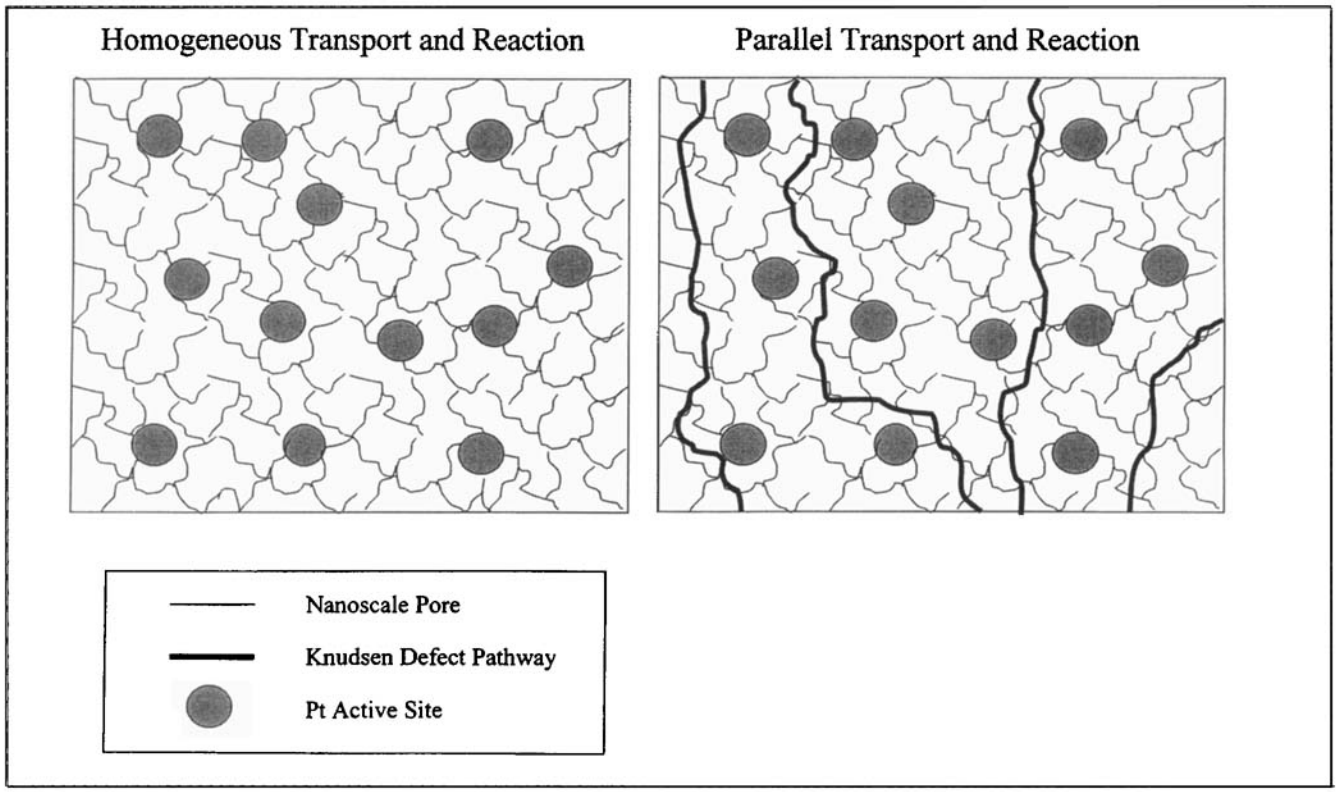

Figure 17. Homogeneous and isotropic pore structures leading to differences in ordering reaction and transport within the membrane.

b_i^o = Langmuir parameter preexponential factor, 1/Pa
$\underline{D}$ = intrinsic or Stefan-Maxwell diffusivity matrix, m^2/s
$\underline{\underline{D}}^{\text{Fick}}$ = Fickian transport matrix, m^2/s
D_i = Stefan-Maxwell pure-component surface diffusivity of species i, m^2/s
D_i^o = Stefan-Maxwell pure-component surface diffusivity preexponential factor of species i, m^2/s
$E_{r\times n,i}$ = activation energy for pseudo-first-order hydrogenation rate constant, kJ/mol
$E_{\text{sur},i}$ = activation energy for surface diffusion on membrane surface, kJ/mol
k = pseudo-first-order, hydrogenation rate constant, mol/(g Pt · s · Pa)
N_i = observed steady-state flux of species i, mol/(m^2 · s)
N_{alkane} = observed steady-state flux of product alkane, mol/(m^2 · s)
$p_{h,i}$ = upstream volume partial pressure of olefin i, Pa
$p_{l,i}$ = permeate volume partial pressure of olefin i, Pa
p_o = constant pressure loading applied to the boundary of a membrane at $t = 0$, Pa
$p(t)$ = transient pressure rise of the permeate chamber, Pa
p_{int} = pressure in the permeate chamber at $t = 0$, Pa
q_{sat} = saturation uptake of adsorbate, mol/kg
r_i = rate of hydrogenation of olefin i, mol/(g Pt · Pa · s)
R = ideal-gas constant, J/(mol · K)
t = time of permeation, s
T = temperature of permeation, K
V_{pc} = volume of the permeate chamber, m^3
w = metal loading of the membrane, kg Pt/kg
z = diffusional coordinate, m

Greek letters

$\Delta H_{\text{ads},i}$ = heat of physical adsorption on membrane surface, kJ/mol
δ = carbon film thickness, μm
ϵ = carbon membrane porosity, m^3 void space/m^3 membrane material
Γ = thermodynamic tensor
η = dimensionless diffusional coordinate
τ = time axis intercept of the integral molar flux, s
ρ = carbon density, kg/m^3
θ_i = adsorbed species i on nanoporous carbon membrane
$\theta_{i,o}$ = fractional loading of species i at $Z = 0$ boundary
τ = time-axis intercept of the integral molar flux, s

Subscripts

h = upstream membrane boundary ($\eta = 0$)
l = permeate volume boundary ($\eta = 1$)

Literature Cited

Acharya, M., and H. C. Foley, "Spray-Coating of Nanoporous Carbon Membranes for Air Separation," *J. Memb. Sci.*, **161**, 1 (1999).

Acharya, M., B. A. Raich, H. C. Foley, M. P. Harold, and J. J. Lerou, "Metal-Supported Carbogenic Molecular Sieve Membranes: Synthesis and Applications," *Ind. Eng. Chem. Res.*, **36**, 2924 (1997).

Acharya, M., M. S. Strano, J. Mathews, S. J. L. Billinge, and H. C. Foley, "Simulation of Nanoporous Carbons: A Chemically Constrained Structure," *Phil. Mag. B*, **79**, 1499 (1999).

Alfonso, M. J., A. Julbe, D. Farrusseng, M. Menendez, and J. Santamaria, "Oxidative Dehydrogenation of Propane on V/Al2O3 Catalytic Membranes. Effect of the Type of Membrane and Reactant Feed Configuration," *Chem. Eng. Sci.*, **54**, 1265 (1999).

Armor, J. N., "Catalysis With Permselective Inorganic Membranes," *Appl. Catal.*, **49**, 1 (1989).

Armor, J. N., "Challenges in Membrane Catalysis," *Chemtech*, **22**, 557 (1992).

Armor, J. N., "Applications of Catalytic Inorganic Membrane Reactors to Refinery Products," *J. Memb. Sci.*, **147**, 217 (1998).

Burggraaf, A. J., "Single Gas Permeation of Thin Zeolite (MFI) Membranes: Theory and Analysis of Experimental Observations," *J. Memb. Sci.*, **155**, 45 (1999).

Chihara, K., M. Suzuki, and K. Kawazoe, "Adsorption Rate on Molecular Sieving Carbon by Chromatography," *AIChE J.*, **24**, 237 (1978).

Foley, H. C., "Carbogenic Molecular-Sieves—Synthesis, Properties and Applications," *Microporous Mater.*, **4**, 407 (1995).

Foley, H. C., D. S. Lafyatis, R. K. Mariwala, G. D. Sonnichsen, and L. D. Brake, "Shape-Selective Methylamines Synthesis—Reaction and Diffusion in a CMS-SiO_2-Al_2O_3 Composite Catalyst," *Chem. Eng. Sci.*, **49**, 4771 (1994).

Harold, M. P., V. T. Zaspalis, K. Keizer, and A. J. Burggraaf, "Intermediate Product Yield Enhancement With a Catalytic Inorganic Membrane. 1. Analytical Model for the Case of Isothermal and Differential Operation," *Chem. Eng. Sci.*, **48**, 2705 (1993).

Kane, M. S., J. F. Goellner, H. C. Foley, R. DiFrancesco, S. J. L. Billinge, and L. F. Allard, "Symmetry Breaking in Nanostructure Development of Carbogenic Molecular Sieves: Effects of Morphological Pattern Formation on Oxygen and Nitrogen Transport," *Chem. Mater.*, **8**, 2159 (1996).

Krishna, R., B. Smit, and T. J. H. Vlugt, "Sorption-Induced Diffusion-Selective Separation of Hydrocarbon Isomers Using Silicalite," *J. Phys. Chem. A*, **102**, 7727 (1998).

Krishna, R., and L. J. P. Vandenbroeke, "The Maxwell-Stefan Description of Mass-Transport Across Zeolite Membranes," *Chem. Eng. J. Biochem. Eng. J.*, **57**, 155 (1995).

Krishna, R., T. J. H. Vlugt, and B. Smit, "Influence of Isotherm Inflection on Diffusion in Silicalite," *Chem. Eng. Sci.*, **54**, 1751 (1999).

Krishna, R., and J. A. Wesselingh, "Review Article Number 50—The Maxwell-Stefan Approach to Mass Transfer," *Chem. Eng. Sci.*, **52**, 861 (1997).

Lafyatis, D. S., "The Design and Synthesis of Carbon Molecular Sieve Catalysts for Shape Selective Catalysis," PhD Thesis, Dept. of Chemical Engineering, Univ. of Delaware, Newark, p. 113 (1992).

Lafyatis, D. S., and H. C. Foley, "Molecular Modeling of the Shape Selectivity for the Fischer-Tropsch Reaction Using a Trifunctional Catalyst," *Chem. Eng. Sci.*, **45**, 2567 (1990).

Mariwala, R. K., and H. C. Foley, "Calculation of Micropore Sizes in Carbogenic Materials from the Methyl-Chloride Adsorption-Isotherm," *Ind. Eng. Chem. Res.*, **33**, 2314 (1994).

Miura, K., J. Hayashi, T. Kawaguchi, and K. Hashimoto, "A Shape-Selective Catalyst Utilizing a Molecular Sieving Carbon with Sharp Pore Distribution," *Carbon*, **31**, 667 (1993).

Raich, B. A., and H. C. Foley, "Supra-Equilibrium Conversion in Palladium Membrane Reactors—Kinetic Sensitivity and Time-Dependence," *Appl. Catal. A—General*, **129**, 167 (1995).

Raich, B. A., and H. C. Foley, "Ethanol Dehydrogenation With a Palladium Membrane Reactor: An Alternative to Wacker Chemistry," *Ind. Eng. Chem. Res.*, **37**, 3888 (1998).

Reyes, P., M. Oportus, G. Pecchi, R. Frety, and B. Moraweck, "Influence of the Nature of Platinum Precursor on the Surface Properties and Catalytic Activity of Alumina-Supported Catalysts," *Catal. Lett.*, **37**, 193 (1996).

Saracco, G., H. Neomagus, G. F. Versteeg, and W. P. M. van Swaaij, "High-Temperature Membrane Reactors: Potential and Problems," *Chem. Eng. Sci.*, **54**, 1997 (1999).

Saracco, G., and V. Specchia, "Catalytic Inorganic-Membrane Reactors—Present Experience and Future Opportunities," *Catal. Rev.—Sci. Eng.*, **36**, 305 (1994).

Saracco, G., G. F. Versteeg, and W. P. M. Vanswaaij, "Current Hurdles to the Success of High-Temperature Membrane Reactor," *J. Mem. Sci.*, **95**, 105 (1994).

Schmitt, J. L., "Carbon Molecular-Sieves as Selective Catalyst Supports—10 Years Later," *Carbon*, **29**, 743 (1991).

Schmitt, J. L., and P. L. Walker, "Carbon Molecular Sieve Supports for Metal Catalysts: I. Preparation of the System—Platinum Supported on Polyfurfuryl Alcohol Carbon," *Carbon*, **9**, 791 (1971a).

Schmitt, J. L., and P. L. Walker, "Carbon Molecular Sieve Supports for Metal Catalysts: II. Selective Hydrogenation of Hydrocarbons Over Platinum Supported on Polyfurfuryl Alchohol Carbon," *Carbon*, **10**, 87 (1971b).

Shiflett, M. B., and H. C. Foley, "Ultrasonic Deposition of High Selectivity Nanoporous Carbon Membranes," *Science*, **285**, 1902 (1999).

Strano, M. S., and H. C. Foley, "Deconvolution of Permeance Through Supported Nanoporous Membranes," *AIChE J.*, **46**, 651 (2000).

Tachibana, M., "Porous, Metal-Containing Carbonaceous Material," U.S. Patent No. 4,970,189 (1990).

Trimm, D. L., and B. J. Cooper, "Preparation of Selective Carbon Molecular Sieve Catalysts," *Chem. Commun.*, 477 (1970).
Trimm, D. L., and B. J. Cooper, "Propylene Hydrogenation over Platinum/Carbon Molecular Sieve Catalysts," *J. Catal.*, **31**, 287 (1973).
van de Graaf, J. M., M. Zwiep, F. Kapteijn, and J. A. Moulijn, "Application of a Silicalite-1 Membrane Reactor in Metathesis Reactions," *Appl. Catal. A—General*, **178**, 225 (1999a).
van de Graaf, J. M., M. Zwiep, F. Kapteijn, and J. A. Moulijn, "Application of a Zeolite Membrane Reactor in the Metathesis of Propene," *Chem. Eng. Sci.*, **54**, 1441 (1999b).
van de Graaf, J. M., K. Kapteijn, and J. A. Moulijn, "Modeling Permeation of Binary Mixtures Through Zeolite Membranes," *AIChE J.*, **45**, 497 (1999c).
van de Graaf, J. M., F. Kapteijn, and J. A. Moulijn, "Permeation of Weakly Adsorbing Components Through a Silicalite-1 Membrane," *Chem. Eng. Sci.*, **54**, 1081 (1999d).
van den Broeke, L. J. P., W. J. W. Bakker, F. Kapteijn, and J. A. Moulijn, "Binary Permeation Through a Silicate-1 Membrane," *AIChE J.*, **45**, 976 (1999).
Yamamoto, M., K. Kusakabe, J. Hayashi, and S. Morooka, "Carbon Molecular Sieve Membrane Formed by Oxidative Carbonization of a Copolyimide Film Coated on a Porous Support Tube," *J. Memb. Sci.*, **133**, 195 (1997).

Manuscript received Dec. 28, 1999, and revision received June 22, 2000.